DOI: 10.61782/fa.2025.0430

FORUM ACUSTICUM
EURONOISE 2025

HOVERING SMALL-SCALE LOW REYNOLDS NUMBER ROTOR-BEAM SOURCE LOCALIZATION USING BOTH NEARFIELD AND FARFIELD MEASUREMENTS

H. Parisot-Dupuis[1*] **B. Mellot**[1] **N. Gariglio** [1] **F. Méry**[2]

[1] ISAE-SUPAERO, University of Toulouse, Toulouse, France
[2] ONERA, University of Toulouse, Toulouse, France

ABSTRACT

The sound radiation of small-scale low Reynolds number rotor in interaction with a beam is measured in anechoic room in hovering condition. The experimental setup is composed by a farfield acoustic instrumentation, a directivity antenna and an array of 45 microphones, and nearfield acoustic intrumentation, a microphone and an array of 16 microphones located near the rotor and flush-mounted on the beam. Both nearfield and farfield microphones are used to characterize the different rotor-beam noise source components, tonal noise associated to the blade passing frequency (BPF) and its harmonics which increases in the presence of the beam, and high frequency broadband noise. The coherent output power (COP) spectral analysis is also used to obtain sound source maps coherent or anti-coherent with nearfield signals. This methodology is first assessed on loudspeakers in anechoic room before to be applied to the rotor-beam test case. Nearfield and farfield acoustic signatures show similar radiation patterns. Tonal noise components are very coherent with nearfield signals and their evolution along the beam differs between low frequency and high frequency BPF harmonics. The high frequency broadband noise is contrarly anti-coherent with nearfield signals and its evolution along the beam shows a maximum level near the blade tip.

**Corresponding author*: *helene.parisot-dupuis@isae-supaero.fr.*

Keywords: *aeroacoustics, source localization, coherent output power, rotor, UAV*

1. INTRODUCTION

The sound generated by bodies in interaction with an airflow is a concern for many applications, especially for noise pollution due to transportation in cities [1]. Transportation noise present often multiple aeroacoustic sources and/or complex interaction phenomenon with possible correlation between sources. This is the case of new unmanned aircraft systems for which the developement leds to many aeroacoustic studies last years [2–8].

In order to reduce the noise coming from these equipments, it is necessary to understand the physical mechanisms responsible for their generation. An interesting way of improving aeroacoustics noise sources understanding is the use of microphone array measurements associated with source localization methods. Indeed, such approach allows to discriminate the different sources while providing a ranking of each of them for the frequencies of interest. The most famous source localization algorithm is the conventional beamforming (CBF) method developed by Billinglsey et al. [9], which is based on the assumption that the sound field radiated by the sources under study follows a certain source model (uncorrelated monopoles). The principle is to localize the sound sources from farfield microphone array measurements by interpreting the propagation delays measured between each microphone of the array and knowing the source-array distance. Parallely, coherent output power (COP) spectral analysis has been developped and was recently applied to microphone array measurements for denoising or source separation purposes [10–12].

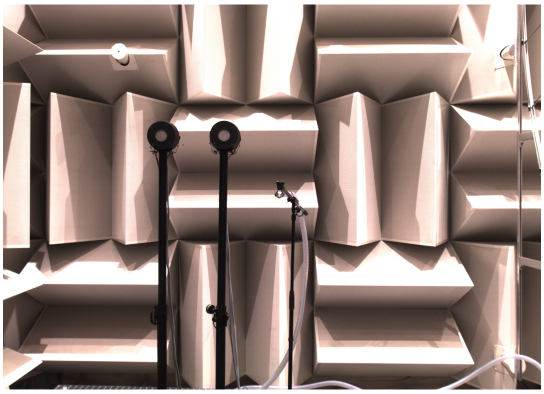

Figure 1. Loudspeakers configuration: S1 (center) and S2 sources (upper left).

This paper proposes to use the degree of coherence of farfield microphone signals with nearfield microphone ones to improve the characterization of complex aeroacoustic noise sources. First, the experimental campaign and associated post processing methodology is presented. Then, the results of preliminary tests on loudspeakers with different degree of coherence are discussed. Finally, the methodology is applied to an aeroacoustic test case: a hovering small-scale low Reynolds number UAV rotor in interaction with a beam.

2. EXPERIMENTAL CAMPAIGN

2.1 Sources configurations

Measurements are performed in ISAE-SUPAERO anechoic room, which is acoustically treated in the frequency range $80 - 16000\ Hz$, and has wedge-tip to wedge-tip dimensions of $5.02 * 5.24 * 5.34\ m^3$ $(L * W * H)$.

A first set of measurements was performed on loudspeakers: a monopolar source Siemens Q-MHF, called $S1$, and two compression drivers BMS 4592, called $S2$. A white noise signal on the frequency range $100-20000\ Hz$ is sended to this three sources. The generation setup allowed to send uncoherent signal, in-phase signal and signals in phase opposition to the two sources $S2$. The positionning of the three sources is shown Figure 1.

A second set of measurements was performed on a hovering small-scale low Reynolds number UAV rotor in interaction with a beam. The rotor has two blades with a NACA0012 blade cross section profile extruded in the radial direction, a constant chord of 0.025 , a constant pitch of $10°$ and a radius $R = 0.1\ m$. The beam is a cylinder

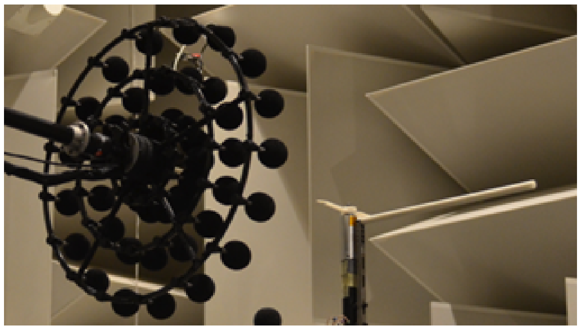

Figure 2. UAV rotor-beam configuration with the 45-channels microphone array.

of diameter $0.02\ m$ and length $0.4\ m$ whose axis is located $0.02\ cm$ below the rotor disk plane. The rotor-beam setup is visible Figure 2 and is described in more details in [6]. Measurements were performed at a rotational speed of $8000\ RPM$.

2.2 Acoustic measurements

The farfield noise radiated by sources is measured by a 2D array of 45 microphones and diameter $0.5\ m$ developed by MicrodB. This array is composed by GRAS 40PH microphones located on 3 concentric circles with irregular spacing (see Figure 2). The array plane was located at a distance of $1\ m$ from the loudspeakers plane and $0.56\ m$ from the rotor-beam setup. For the rotor-beam test case, a directivity antenna of 13 microphones, covering elevation angles $[-60 : 10 : 60]°$, $0°$ being the rotor disk plane, located $1.62\ m$ from the rotor center and perpendicular to the beam was also used. More details about the farfield acoustic instrumentation can be found in [8].

For this study, nearfield measurements were also performed in both cases. The volume acceleration sensor integrated at the exit nozzle of the S1 source is used for the loudspeakers configuration. A microphone GRAS 48LX-1 located on the top of the beam at a distance of $0.8R$ from the rotor axis was used for the rotor-beam configuration. Additionally, a small array of 16 MEMs microphones ICS-40619 was developed to study specifically to study nearfield noise. MEMs were located any $0.005\ m$ between $0.35R$ and $1.1R$ and positionned at the top of the beam instead of the nearfield microphone for some measurements.

Both data acquisition and post-processing were perfomed using Siemens Simcenter Testlab software. Measurements were performed at a sampling frequency of $51.2\ kHz$ during $16.16\ s$. The fast Fourier transform (FFT) on those signals was computed with a Hanning window applied on 100 segments and a sample overlap of 50%, leading to a frequency resolution of $3.125\ Hz$. Source maps have been computed with a sample overlap of 50% for FFT in order to have a frequency resolution of $10\ Hz$ with a source grid cells of size $0.01\ m$.

3. METHODOLOGY

3.1 Conventional beamforming

The conventional beamforming source localization algorithm is based on the propagation delays measured between each microphones that are related to the source-microphone distance. It uses the cross-spectral matrix C, which contains microphones auto-spectra on its diagonal and cross-spectra outside its diagonal, and the free space Green's function g to estimate the sources' position and amplitude q in Pa^2 from the farfield sound pressure measurements p':

$$q = \frac{g^H C g}{||g||^4} \quad \text{with} \quad g = \frac{e^{jkr}}{r} \quad \& \quad C = p'p'^H \tag{1}$$

where ^{H} the complex conjugate transpose, j the imaginary unit, k the wavenumber and r the distance between microphones and focal points.

The cross-spectral matrix diagonal removal technique is used for maps averaging computation to obtain a single acoustic map from a time selection including multiple FFT time segments, while removing the noise contained associated to microphones auto-spectra. This allows to obtain source maps for each frequency or frequency range of interest.

3.2 Coherence with nearfield data

When reference data are available near sources they can be used to separate the different sources' contributions at other microphone's locations. This can be done by calculating the coherent or anti-coherent output power (COP or ACOP) spectra [10]:

$$COP_{rm} = \gamma_{rm}^2 * S_{mm} \tag{2}$$

$$ACOP_{rm} = (1 - \gamma_{rm}^2) * S_{mm} \tag{3}$$

with

$$\gamma_{rm}^2 = \frac{|S_{rm}|^2}{S_{rr} * S_{mm}} \tag{4}$$

where γ_{rm} and S_{rm} are respectively the coherence and the cross-power between a microphone, denoted m, and the nearfield reference signal, denoted r, and S_{mm} and S_{rr} arer respectively the auto-spectra of the microphone and the reference signal. This methodology was used recently to denoise microphone array signals or to separate different noise source contributions [11, 12].

Reference nearfield data can also be used to distinguish different sources' contributions on beamforming source maps. This is obtained using the COP and ACOP principles by weighting microphone averaged auto-spectra S_{mm} and by adding a phase relationship related to this reference:

$$S'_{mm} = COP_{rm} * \frac{{S_{rm}}^2}{|S_{rm}|^2} \quad \text{or} \quad ACOP_{rm} * \frac{{S_{rm}}^2}{|S_{rm}|^2} \tag{5}$$

The beamforming processing is then applied to those new microphone averaged autospectra S'_{mm}, to obtain source maps coherent or anti-coherent with the reference signal.

3.3 Assessment on loudspeaker test case

Measurements were performed with the three loudspeakers in three cases: sources S2 uncoherent, coherent in phase and coherent in phase opposition. Coherent and anti-coherent beamforming maps are then obtained by using S1 volume acceleration sensor as reference.

As expected, the coherent beamforming map obtained for the case of three uncoherent sources highlights the source S1, whereas the anti-coherent beamforming maps highlights S2 sources. This allows to identify the contribution of the source S1 even if its amplitude is lower. Figure 3 shows as example source maps obtained at $2000\ Hz$. Symbols indicate sources locations, S1 source being at the center. Others cases are not presented here but confirmed the ability of the methodology to separate coherent and anti-coherent sources contributions.

4. ROTOR-BEAM NOISE CHARACTERIZATION

4.1 Farfield spectra

Previous papesr shows that the rotor noise is characterized by tonal noise at the blade passing frequency (BPF) and its harmonics as well as a high frequency broadband noise (BBD), and that the presence of the beam increases the magnitude of BPF harmonics leading to a hump with a maximum level around $5 * BPF$ [4, 6].

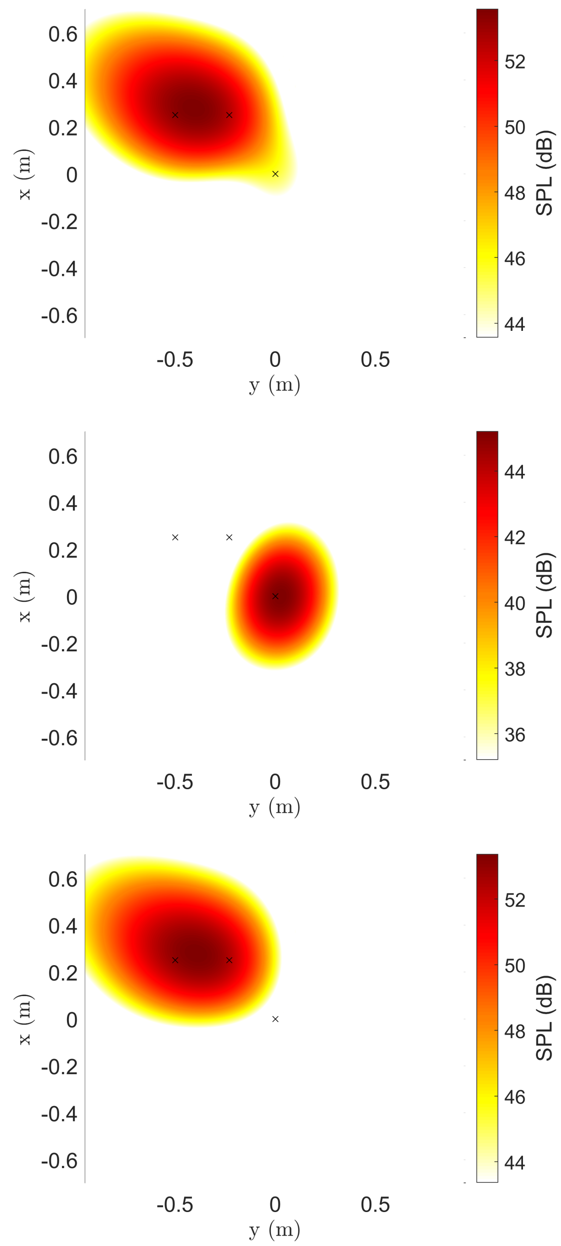

Figure 3. Maps obtained for 3 uncoherent sources at 2000 Hz: CBF (top), coherent CBF (center) & anti-coherent CBF (bottom).

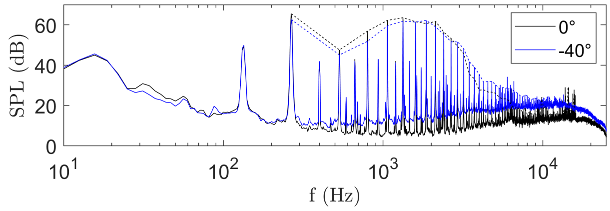

Figure 4. Spectra obtained for rotor-beam in the rotor disk plane $0°$ & toward the ground $-40°$.

A numerical study [8] showed that the BPF harmonics increase seems to be mainly due to the beam radiation, suggesting a noise generation mechanism related to unsteady loading when the blade passes above the beam. Figure 4 highlights those noise components, with the hump of BPF harmonics and the impact of the elevation angle on the high BPF harmonics and broadband noise levels.

4.2 Source maps

Source maps were here obtained using conventional beamforming based on fixed sources to focus on the intetaction noise with the array plane parallel to the beam as described in [8]. Coherent and anti-coherent source maps targeting the different noise components have been computed taking nearfield microphone on the beam as reference sensor. Locations of the rotor, the beam and the test stand are indicated by black lines on the source maps. To complete the source maps, farfield directivity diagrams with and without coherent or anti-coherent with the reference beam microphone are plotted for tonal components $5 * BPF$, $22 * BPF$ and the high frequency broadband noise (BBD) Figure 5.

For the highest BPF harmonic of the hump, $5 * BPF$, the CBF source map is identical to the CBF source map coherent with the beam nearfield microphone, whereas the anti-coherent source map is several orders of magnitudes below. This confirms the relationship between this BPF harmonic level and the periodic blade passing above the beam, and source maps indicate an omnidirectional radiation which corresponds to the farfield directivity perpendicular to the beam (see Figure 5).

Then, it was chosen to study the BPF harmonic $22 * BPF$ which corresponds to a frequency for which the tonal level is decreasing but the broadband level is increasing. In this case, source maps highlight that the main source remains here the one coherent with the beam

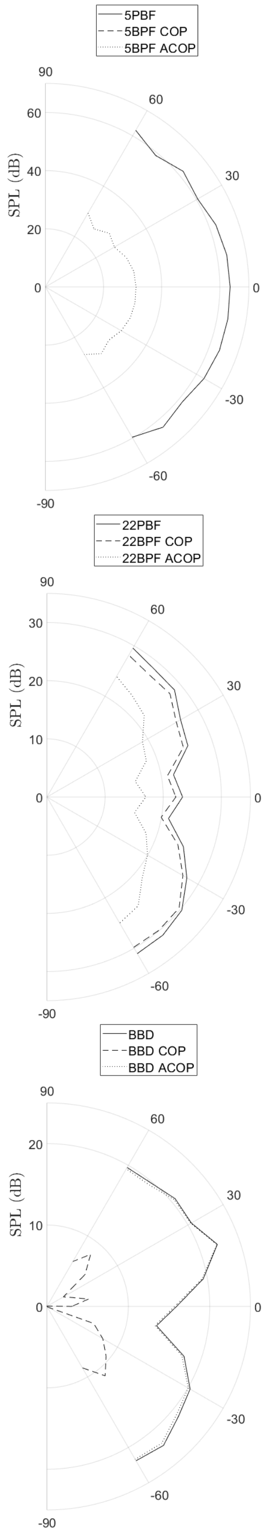

Figure 5. Farfield directivity obtained for rotor-beam at $5*BPF$, $22*BPF$ & BBD with and without coherent or anti-coherent weighting with nearfield data.

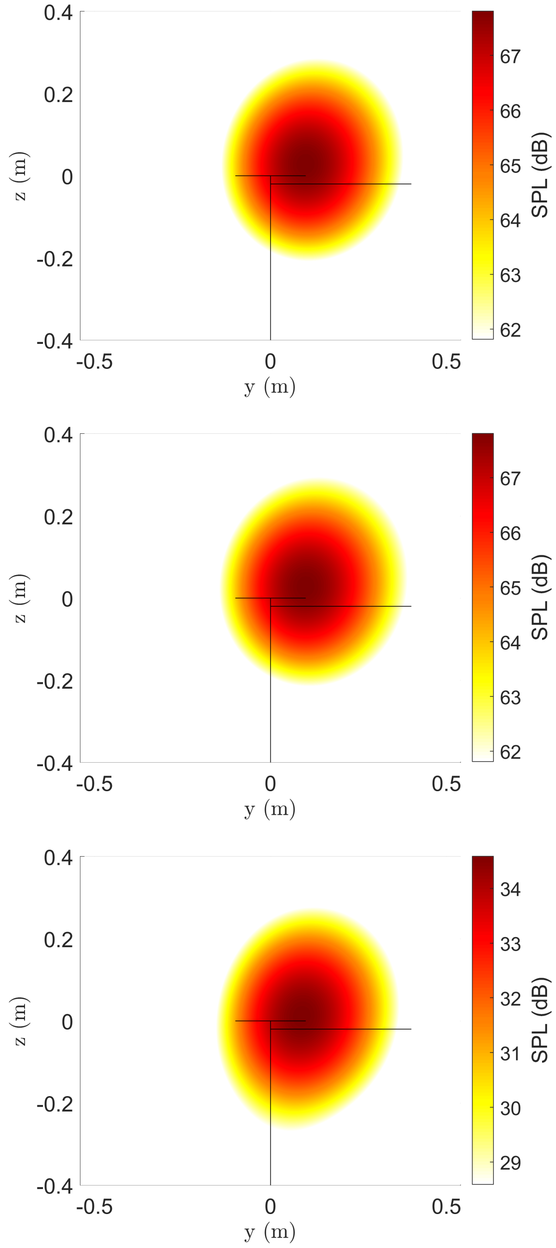

Figure 6. Source maps obtained for rotor-beam at 5*BPF: CBF (top), coherent CBF (center) & anti-coherent CBF (bottom).

nearfield microphone, but the anti-coherent source map allows to identify another source component slightly lower in terms of level and with a different radiation pattern. Looking at the corresponding farfield directivity (Figure 5) we can see that both noise components seem to dipole-like patterns.

Finally, the high frequency broadband noise in the frequency region without tones is studied (frequency of 13000 Hz was chosen). For this noise component we can observe that source map is entirelly determined by the anti-coherent source map, confirming that the sources anti-coherent with the reference beam microphone are associated to the broadband part of the spectrum. The shape of the corresponding source maps indicates a dipolar radiation, as well as the directivity diagrams Figure 5, which is consistent with the trailing edge broadband noise directivity previously identified [6].

4.3 Noise components evolution along the beam

Additionnally, the MEMs linear array was used to plot sound pressure levels (SPL) evolution of each noise component along the beam. COP and ACOP SPL evolutions respect to the MEMs located at $0.8R$ to be consistent with the beam nearfield microphone location.

For the main BPF harmonic an increase along the beam is observed with a maximum at $0.9R$ which is consistent with previous numerical simulation results, and the coherence of this phenomenon with the reference MEMs is confirmed. A previous numerical study showed that the beam was the main contributor to the farfield noise radiation at this BPF harmonic and that the main beam radiating area was around $80 - 90\%$ of the blade radius [7], which is similar to the maximum level location. The $22 * BPF$ harmonic present a diffrent behaviour with a first increase until $0.6R$, then a minimum, and after a second increase with a maximum at $0.95R$, with again the part coherent with the reference MEMs being the main one.

In the case of the high frequency broadband noise the evolution is quite flat between $0.4R$ and $0.9R$ and a peak is observed at $1.05R$. The level of this noise component along the beam is mainly anti-coherent with the reference MEMs but the trend along the beam is the same for both coherent and anti-coherent parts. Anti-coherent parts of tonal noise components present very similar behaviour with a peak at $1R$. The location of those peaks seems to suggest that this noise component might be due to blade tip wake impingement on the beam.

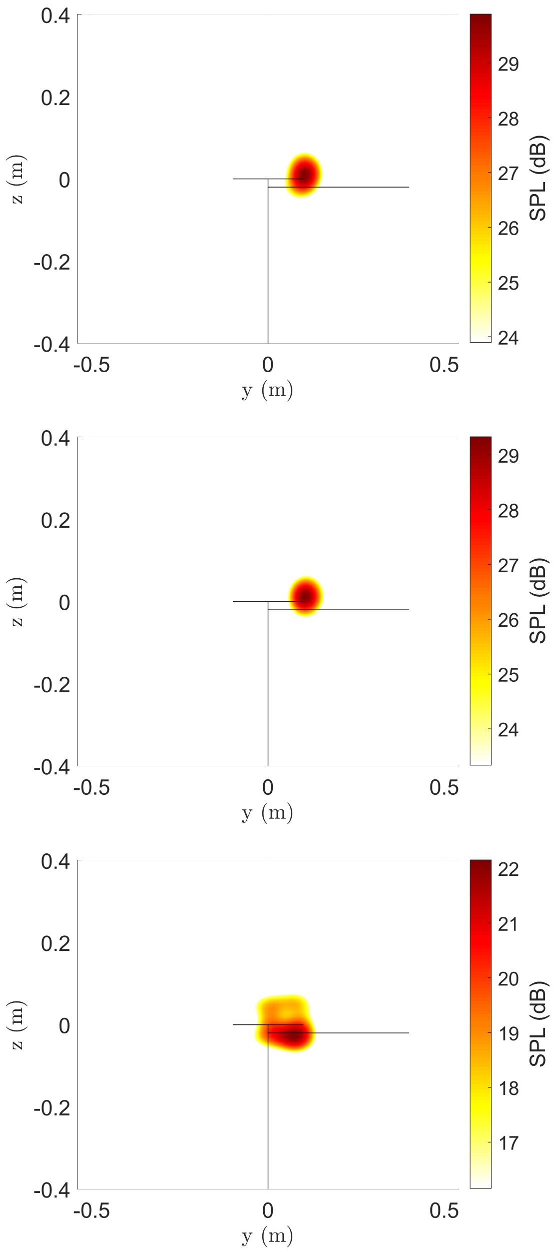

Figure 7. Source maps obtained for rotor-beam at 22*BPF: CBF (top), coherent CBF (center) & anti-coherent CBF (bottom).

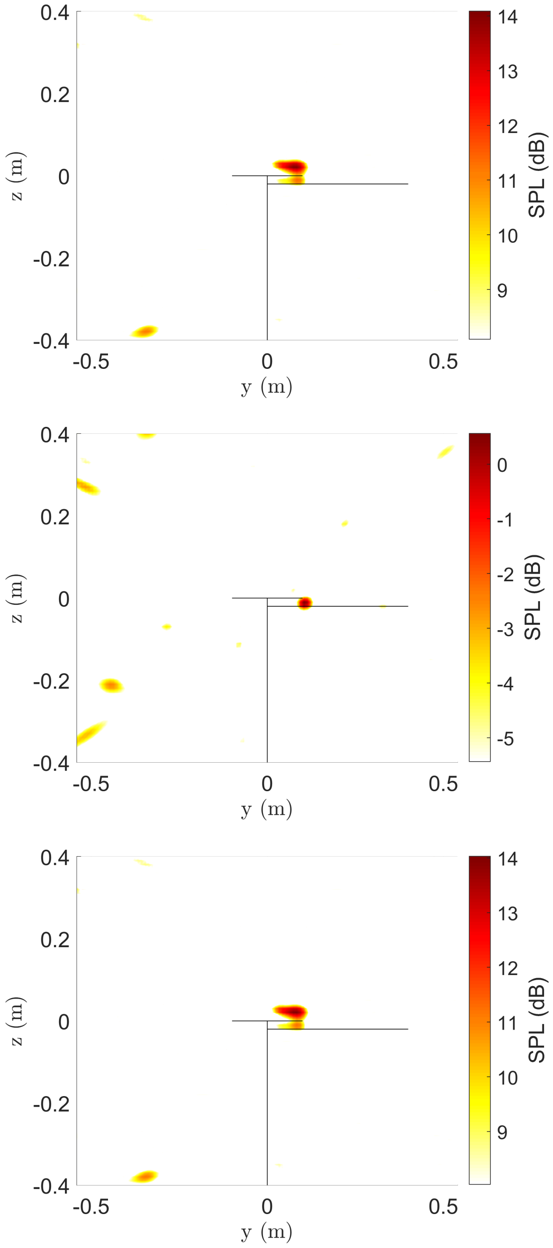

Figure 8. Source maps obtained for rotor-beam at BBD: CBF (top), coherent CBF (center) & anti-coherent CBF (bottom).

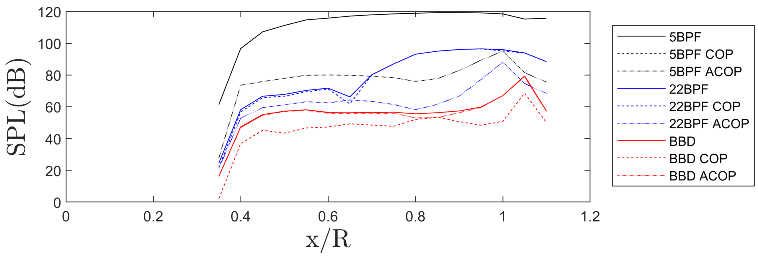

Figure 9. SPL along the beam for $5 * BPF$, $22 * BPF$ & BBD: total, coherent & anti-coherent with the MEMs located at $0.8R$.

5. CONCLUSIONS

Microphone array measurements were performed in anechoic room synchroneously with other acoustic nearfield and farfield measurements in order to help the identification of the different noise components associated to complex aeroacoustic sources. The proposed methodology is to compute beamforming source maps coherent or anti-coherent with nearfield reference signals using the coherent output power (COP) spectral analysis.

Preliminary tests on loudspeakers with different degree of coherence were first performed. The ability of the proposed methodology to distinguish source contributions coherent or anti-coherent with a nearfield reference signal was demonstrated, even when there is a significative difference of levels between the two contributions.

The methodoloy was then applied to an areoacoustic test case: a hovering small-scale low Reynolds number UAV two-bladed rotorof diameter $0.2\ m$ and NACA0012 blade profile in interaction with a cylindrical beam of diameter $0.02\ m$. Previous studies showed tonal noise at the blade passing frequency (BPF) and its harmonics, increased by the presence of the beam with a maximum around $5 * BPF$, and high frequency broadband noise.

Conventional beamforming was used to obtain source maps coherent and anti-coherent with a nearfield microphone located on the beam at 80% of the blade radius. The strongest BPF harmonic appeared to be coherent with the beam nearfield microphone, confirming the relationship between this BPF harmonic level and the periodic blade passing above the beam. High frequency BPF harmonics in the frequency region where the broadband increases appeared to be coherent with the beam nearfield microphone too, but another anti-coherent source with a dipolar radiation pattern and lower level was also identified. The high frequency broadband noise is contrarly perfectly anti-coherent with the beam nearfield microphone with a dipolar radiation pattern associated to trailing edge noise. Farfield directivity diagrams coherent or anti-coherent with the beam nearfield microphone allowed to confirm the radiation patterns visibles on source maps.

Additionally, a linear MEMs array located on the beam was used to determine the sound pressure levels (SPL) evolution of each noise component along the beam, coherent and anti-coherent respect to the MEMs located at 80% of the blade radius. The evolution of the low frequency BPF harmonic level along the beam leads to one hump coherent with the reference MEMs, whereas the one of the high frequency BPF harmonic leads to two humps also coherent with the reference MEMs. For the high frequency broadband noise a flat evolution, mainly anti-coherent with the reference MEMs, with a maximum level near the blade tip is found.

Complementary post processing are planned and this methodology will be also used to study the different noise source components evolution with the rotational speed, the beam diameter, and the rotor-beam distance. It is also envisaged to apply it to more realistic configurations: different airflow conditions, rotor-airframe and/or multiple rotors interactions for instance.

6. ACKNOWLEDGMENTS

The authors gratefully acknowledge financial support from the French Defense Procurement Agency (DGA). They are grateful to ISAE-SUPAERO technical staff for their contribution to the experimental campaign.

7. REFERENCES

[1] C. Marquis-Favre, E. Premat, and D. Aubrée, "Noise and its effects - a review on qualitative aspects of sound. part ii: Noise and annoyance.," *Acta Acust united Ac*, vol. 91, no. 17, pp. 626–642, 2005.

[2] N. Zawodny, D. Boyd, and C. Burley, "Acoustic characterization and prediction of representative, small-scale rotary-wing unmanned aircraft system components," in *In Proc. of the American Helicopter Society (AHS) 72nd Annual Forum*, pp. 16–19, 2016.

[3] N. Zawodny and D. Boyd, "Investigation of rotorairframe interaction noise associated with small-scale rotary-wing unmanned aircraft systems," in *In Proc. of the American Helicopter Society (AHS) 73rd Annual Forum*, 2017.

[4] R. Gojon, T. Jardin, and H. Parisot-Dupuis, "Experimental investigation of low reynolds number rotor noise," *The Journal of the Acoustical Society of America*, vol. 149, no. 6, pp. 3813–3829, 2021.

[5] Y. Wu, M. Kingan, and S. Go, "Propeller-strut interaction tone noise," *Physics of Fluids*, vol. 34, pp. 3813–3829, 2022.

[6] R. Gojon, H. Parisot-Dupuis, B. Mellot, and T. Jardin, "Aeroacoustic radiation of low reynolds number rotors in interaction with beams," *The Journal of the Acoustical Society of America*, vol. 154, no. 2, p. 1248–1260, 2023.

[7] N. Doué, R. Gojon, and T. Jardin, "Numerical investigation of the acoustics radiation of a two-bladed rotor in interaction with a beam," in *In Proc. of Numerical investigation of the acoustics radiation of a two-bladed rotor in interaction with a beam*, 2023.

[8] H. Parisot-Dupuis, R. Gojon, and N. Doué, "Feasibility of hovering small-scale low reynolds number rotor-beam source localization by microphone array measurements," in *In Proc. of 30th AIAA/CEAS Aeroacoustics Conference*, p. 3063, 2024.

[9] J. Billinsgley and R. Kinns, "The acoustic telescope," *J. Sound Vib.*, vol. 48, no. 4, pp. 485–510, 1976.

[10] W. G. Halvorsen and J. S. Bendat, "Noise source identification using coherent output power spectra," *Journal of Sound and Vibration*, vol. 9, no. 8, pp. 15–24, 1975.

[11] P. Sijtsma, M. Dreux, B. Delescluse, R. Leneveu, and J. Mardjono, "Coherent output power with groups of microphones," in *30th AIAA/CEAS Aeroacoustics Conference (2024)*, (Rome, Italy), p. 3330, 2024.

[12] N. Auquier, J. Cuenca, and L. D. Ryck, "Coherence-based nearfield acoustic holography for damage detection in plates," in *In Proc. of ISMA*, pp. 2899–2907, 2020.